Channeling macrophage polarization by using a selective translation inhibitor

Sujoy Chatterjee[1], Emily Waligurski[1], Bidisha Bhattacharya[1], Shivraj Mohanrao Yabaji[1], Nandini Vallavoju[2], Somak Roy[4], Lauren E. Brown[2], Aaron B. Beeler[2], Alexander R. Ivanov[4], Lester Kobzik[3], John A. Porco Jr[2], and Igor Kramnik*[1]

[1]Pulmonary Center, Department of Medicine, Boston University School of Medicine, National Emerging Infectious Diseases Laboratories (NEIDL), Boston University, Boston MA, 02118, USA

[2]Department of Chemistry, Center for Molecular Discovery (BU-CMD), Boston University, Boston, MA, 02215, USA

[3]Department of Environmental Health, Harvard School of Public Health, Boston, MA, 02115, USA

[4]Barnett Institute of Chemical and Biological Analysis, Department of Chemistry and Chemical Biology, Northeastern University. Boston, MA, 02115, USA

* Corresponding author, Email: ikramnik@bu.edu

Running title: Macrophage polarization using rocaglates

Abstract

The increasing problem of infectious diseases caused by antibiotic-resistant bacteria has intensified a search for novel host-directed therapies aimed at either boosting immune-mediated bacterial control or reducing immunopathology. Macrophages play central roles in eliminating pathogens as well as in tissue homeostasis and repair via alternative activation programs, M1-like and M2-like, respectively. Macrophages of both phenotypes are often present at the sites of chronic unresolved inflammation, such infectious granulomas and solid tumors, where the M2-like macrophages generate microenvironment conducive for pathogen survival or tumor progression.

Interferon-gamma is a major cytokine that drives M1-like macrophage activation, which is essential for control of intracellular bacterial pathogens. To evaluate M1-like macrophage polarization as a broad therapeutic strategy, we searched for small molecules capable of enhancing effects of low concentrations of IFNγ on M1 macrophage polarization. We identified synthetic rocaglates that potentiated macrophages responses to low concentrations of IFNγ. Although known as potent translation inhibitors in tumor cell lines, in primary macrophages select rocaglates induced the upregulation of IRF1, a master regulator of IFNγ -activated pathways, stimulated autophagy and increased macrophage resilience to oxidative stress. In contrast, rocaglates inhibited macrophage responsiveness to IL-4, a prototypical activator of the M2-like phenotype. The M1-like macrophage programing by rocaglates was mechanistically linked to selective translation inhibition and modulation of MAP kinase network.

Thus, rocaglates represent a novel class of immunomodulators that can enforce macrophage polarization towards the M1-like phenotype in complex microenvironments

associated with hypofunction of type 1 and/or hyperactivation of type 2 immunity, e.g., chronic bacterial infections, allergies and, possibly, certain tumors.

Introduction

The increasing problem of infectious diseases caused by antibiotic-resistant bacteria has intensified a search for novel therapeutic approaches. Among them are host-directed therapies aimed at either boosting immune-mediated bacterial control or reducing immunopathology, broadly referred to as mechanisms of host resistance or disease tolerance, respectively (*1*). Many intracellular bacterial pathogens reside in macrophages, the very cells of innate immune system whose major function is to eliminate invading pathogens. This paradox is enabled by macrophages' plasticity, which successful pathogens exploit to create cellular niches for persistence and replication within inflamed tissue of susceptible hosts.

To combat intracellular bacteria, macrophages activate cell autonomous defense mechanisms, such as phagocytosis, production of highly toxic reactive oxygen and nitrogen species, bactericidal peptides, as well as phagosome maturation and autophagy to deliver the ingested pathogens to lysosomes for destruction. This pro-inflammatory type of macrophage activation can be induced by microbial ligands and proinflammatory cytokines. It is broadly referred to as "classical" or M1 type, although this definition encompasses an array of related, but non-identical macrophage activation states. Individuals whose macrophages that fail to respond to IFNγ, the prototypical M1 differentiating signal, are extremely susceptible to infections caused by intracellular mycobacterial species, including an avirulent vaccine strain of *M.bovis* BCG and a normally avirulent non-tuberculous mycobacteria (NTM).The alternative macrophage activation programs, broadly referred to as M2 type, are mediated by upregulation of anti-inflammatory cytokines and characterized by an increased macrophage permissiveness for intracellular bacteria. Activation of an alternative macrophage activation program, M2 type, by IL-4 favors *M.tb* replication by suppressing autophagy and antigen presentation by the infected macrophages. Overexpression of IL-4 in a mouse model in vivo leads to progression of tuberculosis (TB) and formation of organized necrotic granulomas typical of human TB(*2*). The

M2-like differentiation of macrophages is also involved in local immune suppression within tumor microenvironments and tumor promotion (*3*). However, the M2-like macrophages play important homeostatic and adaptive physiological roles in immune regulation, tissue remodeling, fibrosis and control of parasitic helminth infections(*4*). Thus, within specific in vivo environments macrophages may be exposed to multiple and often conflicting polarization signals. For example, a helminth-induced type 2 immune response antagonizes host protective responses to mycobacteria(*5*).

In vitro, the prototypic M1- and M2-like macrophage polarization states can be artificially induced by treatment with cytokines or microbial ligands and represent polar antagonistic phenotypes. Thus, pretreatment with IL-4 was shown to downregulate the macrophage responsiveness to IFNγ (*5-9*) , while priming with IFNγ reduces their responses to IL-4(*10*). Despite the antagonism of the macrophage polarization programs, recent studies demonstrated simultaneous presence of M1- and M2-like macrophages within TB lesions(*11, 12*) and suggested that the balance of M1/M2 macrophage phenotypes locally within TB lesions may determine trajectories of the individual granuloma progression(*13*). Spatial transcriptomic analysis and immunochemistry revealed that the M2-like macrophage markers were more abundant within the inner areas of TB granulomas (*11, 12*), whereas the IFNγ-producing T cells were located mostly on the periphery of the organized granulomas(*14*). Because IFNγ is a labile homodimer, the diffusion of its biologically active form within inflammatory lesions is limited(*15*)(. Thus, in vivo the macrophage polarization is influenced not only by systemic cytokine levels, but also by the composition and anatomy of specific lesions, such as TB granulomas or tumors. To evaluate M1-like macrophage polarization as a broad therapeutic strategy, we searched for small molecules capable of enhancing effects of low concentrations of IFNγ on M1 macrophage polarization. We surmised that these compounds would boost macrophage differentiation towards the M1-like phenotype locally at the sites where IFNγ is produced upon pathogen recognition. Using an original screening strategy in

vitro, we identified synthetic rocaglates that potentiated macrophages responses to low concentrations of IFNγ (*16*). Rocaglates are a class of bioactive derivatives of natural products isolated from medicinal plants of the *Aglaia* species that have been used in traditional Chinese medicine for treatment of fever, cough, diarrhea and inflammation. In modern medicine, the therapeutic potential of synthetic rocaglates has been evaluated for cancer therapy(*17-20*). Rocaglates bind to and suppress the RNA helicase activity of the eIF-4A subunit of the eIF4F translation initiation complex and inhibit cap-dependent protein translation (*17, 21*). Also, the structurally related rocaglamide A (RocA) inhibits the Raf-MEK-ERK growth factor activated pathway by targeting prohibitin 1 and 2(*22*).

Although known as potent translation inhibitors in tumor cell lines, we found that in primary macrophages select rocaglates induced the upregulation of IRF1, a master regulator of IFNγ -activated pathways. Increased levels of IRF1 mRNA and protein were seen in rocaglate-treated bone marrow-derived macrophages (BMDMs) primed with low concentrations of IFNγ (0.1 U/ml). In the present study, we delineate the mechanism of macrophage activation by rocaglates. We find that rocaglates channel macrophage differentiation towards the M1-like phenotype through their synergy with IFNγ, and by their inhibition of macrophage responsiveness to IL-4. Thus, rocaglates represent a novel class of immunomodulators that may be particularly useful for diseases associated with hypofunction of type 1 and/or hyperactivation of type 2 immunity, e.g., chronic bacterial infections, allergies and, possibly, certain tumors.

Results

Macrophage activation by rocaglates is coupled to partial translational inhibition

To delineate the relationship between translation inhibition and macrophage activation by rocaglates, we screened a library of synthetic rocaglate derivatives. Out of 86 compounds, twenty-three induced significant IRF1 mRNA upregulation in the presence of 0.2 U/ml of IFNγ. Next, we determined the translation inhibitory concentrations IC_{50} of these compounds using the 293TR-FLuc translation reporter cell line (*17*). We observed a tight negative correlation (r = -0.6832) between the IRF1 mRNA induction and IC_{50} of those compounds (**Fig.1A, Supplementary Table 1**) demonstrating mechanistic link between the translational inhibition and IRF1 co-stimulation properties. To verify this relationship in primary macrophages, first we compared translation inhibition activities of two structurally similar rocaglates CMLD010536 and CMLD010850 (**Fig.1B**) in mouse bone marrow-derived macrophages (BMDM) using a puromycin incorporation assay (**Fig 1 C**)(*23*). CMLD010536 exerted greater translation inhibition than CMLD010850 in primary macrophages. Next, we compared the induction of target genes by these compounds (**Fig.1D**): CMLD010536 was significantly more potent as an inducer of IRF1 mRNA expression cooperatively with low dose of IFNγ, as well as of another, IFNγ-independent, rocaglate target gene TXNIP (*17*).

Taken together these data demonstrate that macrophage activation by rocaglates is proportional to their translation inhibition activity. Importantly, general translational inhibitors, such as cycloheximide and puromycin, do not cause IRF1 co-stimulation, described in our previous studies (*16*).

Activation of p38 stress kinase and integrated stress response pathways mediate the macrophage activation by rocaglates

To further investigate the dynamics of translation inhibition by CMLD010536 in BMDM, we used a puromycin incorporation assay. Puromycin incorporation during a one-hour pulse was determined after 2 - 24 h of rocaglate treatment by western blot using puromycin-specific antibodies. The rocaglate treatment significantly reduced translation rates at all timepoints in a dose-dependent manner (**Fig.2A**). However, the levels of ongoing translation were similar at all of the timepoints demonstrating that translation inhibition was partial and sustained over the time course of the rocaglate treatment. To identify proteins expressed in BMDMs after 24 h of treatment with 100 nM of CMLD010536, we performed proteomic analysis using mass spectrometry (**Supplemental Table 2**). The abundance of Sequestosome 1 (SQSTM1 aka p62) protein was found to significantly increase. We confirmed the induction of p62 protein and mRNA (**Figs.2B&C),** demonstrating that treatment of BMDM with the rocaglate induced de novo p62 protein synthesis.

The SQSTM1/p62 protein plays an important role in stress resilience by controlling selective autophagy and anti-oxidant defense gene expression (*24-33*). Its expression can be induced by various stressors. Our previous analysis of CMLD010536-activated pathways using gene expression profiling suggested activation of stress kinase-mediated pathways(*16*). Therefore, we tested whether the p62 induction by CMLD010536 is mediated by stress-activated MAP kinases. The p38 inhibitor (SB203580 at10 uM) added 30 min prior to treatment with 100 nM CMLD010536 completely abrogated the p62 mRNA upregulation. The effect of the JNK inhibitor (SB600125) was less prominent, while ERK inhibitor (U0126/PD98059) had no effect (**Fig.2D**). We also observed a dramatic downregulation of another rocaglate-inducible mRNA, Ptgs2 (**14.** Bhattacharya et al., 2016) by the p38, but not by the JNK or ERK inhibitors (**Supplemental Fig.1**) confirming the role of p38 MAPK in rocaglate-inducible gene expression.

Next, we compared the kinetics of p38 phosphorylation (**Fig.2E**) and p62 mRNA upregulation (**Fig.2F**) during the course of the rocaglate treatment. We observed rapid activation

of p38, which started at 15 min of the treatment, reached a plateau at 30 – 120 min and declined by 4 h. Meanwhile, the p62 mRNA continued to increase 4 – 24 h of the treatment duration. Because p38 activation can be induced by reactive oxygen species (ROS), we tested whether oxidative stress plays a role in p62 induction by the rocaglate. However, p62 mRNA induction was unaffected in the presence of ROS scavenger N-acetyl-cysteine (NAC) (**Fig.2G**). Comparing the p62-inducing activities of CMLD010536 with natural rocaglates silvestrol and rocaglamide A demonstrated that those compounds had similar activities in this assay, while CMLD010850 did not induce p62 induction (**Fig.2H**). This observation is consistent with the importance of translation inhibitory activities of rocaglates in macrophage activation. Notably, another suppressor of cap-dependent translation rapamycin, which is known to inhibit translation via inhibition of mTOR pathway, as well as the known translation elongation inhibitor cycloheximide, both failed to stimulate p62 gene expression, (**Fig.2I**).

Several stress-activated kinases induce inhibition of cap-dependent translation via phosphorylation of translation initiation factor eIF2A. This initiates a cascade of responses known as the Integrated Stress Response (ISR). ISR initiation and maintenance are mediated by the transcription factors ATF4 and ATF3. The ATF4 translation is initiated upon inhibition of cap-dependent translation, leading to stimulation of ATF3 and other downstream targets. We observed that both ATF4 and ATF3 proteins were upregulated at later timepoints of the CMLD010536 treatment (16 – 24 h, **Fig.2J, Fig.2K, Supplemental Fig.2**).

Our data demonstrate that macrophage treatment with rocaglates induces step-wise transcriptome and proteome remodeling. At the early initiation step (0.5 – 2 h), translation inhibition is associated with the activation of p38 stress kinase that drives transcriptional upregulation of p62, Ptgs2 and, likely other inflammatory genes. The translation of ISR transcription factors and p62 occurs with a delay at a later stage (16 – 24 h) of rocaglate treatment. This is consistent with the known ability of rocaglates to inhibit eIF4A helicase, a component the translation initiation complex. At this later stage, the activating effects of

rocaglates on macrophages mimic diverse stressors whose activities converge on a common stress response module – ISR. In contrast to eIF2A kinases, however, the effect of rocaglates is partial and selective that allows for the upregulation of proteins that activate stress adaptation pathways.

P38 mediates synergy of rocaglates with low concentrations of IFNγ

In the presence of low concentrations of IFNγ, CMLD010536 induces upregulation of IRF1, a key transcription factor in the IFNγ network. The upregulation of the IRF1 gene expression by IFNγ is mediated by the binding of STAT1 homodimers to the gamma-activatable sequence (GAS) in the IRF1 promoter. STAT1 homodimer formation and promoter binding requires STAT1 phosphorylation at the canonical tyrosine-701 by JAK kinases, an event that occurs upon IFNγ binding to its receptor (*34, 35*). However, CMLD010536 increased neither the promoter binding activity of STAT1, nor its phosphorylation at the canonical tyrosine site (data not shown). There is an emerging evidence that serine phosphorylation of STAT1 by stress-activated MAP kinases p38 and JNK may mediate various stress responses (*36*). Thus, Ser-727 phosphorylation of STAT1 accounts for nearly 80% of IFNγ-induced transcriptional activity, but does not mediate STAT1 DNA binding or nuclear translocation (*37-39*). Therefore, we tested whether MAP kinase(s) mediate the synergistic effect of rocaglate on IRF1 induction.

As shown in **Fig.3A**, treatment of BMDMs with the rocaglate alone suppressed IRF1 protein levels. However, in the presence of IFNγ at concentrations as low as 0.05 and 0.1 U/ml, CMLD010536 boosted the levels of IRF1 protein and this effect was abrogated by p38 inhibition. Rocaglate treatment induced p38 phosphorylation in these settings, while low concentrations of IFNγ alone did not (**Fig.3B**). We observed similar effect of the p38 inhibitor on IRF1 mRNA induction (**Fig.3C**), while it had no negative effect on IRF1 mRNA levels induced by increasing

concentrations of IFNγ alone (**Fig.3D**). In addition, we found that CMLD010536 induced STAT1 Ser727 phosphorylation as early as 15 min which was maintained at least up to 4 h (**Fig. 3E**). Thus, we propose a model where low doses of IFNγ are sufficient to initiate STAT1 dimer formation and binding to the IRF1 promoter, while the p38 activation boosts and sustains the IRF1 transcription by enhancing interactions with transcriptional co-activators in a STAT1 Ser-727 dependent manner.

To summarize the findings above, we determined that p38 MAPK pathway activation plays a central role in both IFNγ-dependent and -independent pro-inflammatory macrophage responses induced by rocaglates.

Suppression of the alternative activation of macrophages by rocaglates

We investigated whether activation of the pro-inflammatory (M1-like) program by CMLD010536 could concurrently suppress the alternative (M2-like) macrophage activation by IL-4. In agreement with the antagonistic relationship of these modes of macrophage activation, pretreatment of macrophages with IFNγ abrogated their response to IL-4 (as measured by the Arg1 mRNA induction) in an IFNγ-dose-dependent manner (**Fig.4A, left panel**). Similarly, induction of Arg1 and Fizz1 mRNAs by IL-4 was suppressed by CMLD010536 in a dose-dependent manner (**Fig 4A, middle and right panels**). Interestingly, this suppressor effect of the rocaglate did not require the co-stimulation with IFNγ.

Upregulation of the IL-4-inducible genes is mediated by transcription factor STAT6. To analyze the rocaglate effect on the DNA-binding activity of STAT6, we performed electrophoretic mobility shift assay (EMSA) using a STAT6 consensus sequence oligonucleotide probe (**Fig.4B**). Increased STAT6 binding was readily detected in macrophages stimulated with IL-4 (25 ng/ml) for 4 hs. Pretreatment with 30 and 100 nM of CMLD010536 for 2 h prior to the IL-4 stimulation inhibited STAT6 binding. This effect was associated with neither decrease in the

total, nor in the nuclear, STAT6 protein levels (**Fig.4C** upper and lower panels, respectively). At 100 nM the ability to suppress alternative macrophage activation was displayed only by CMLD010536, silvestrol and rocaglamide A (**Fig.4D**), but not by CMLD010850, which is a less potent translational inhibitor (**Fig 1C**). These observations suggested that translation inhibition was necessary to inhibit STAT6 DNA binding activity, but was not due to reduced STAT6 protein levels, *i.e.* it was a regulatory phenomenon.

We next sought to determine whether the rocaglate suppressor activity was mediated by stress kinases and found that neither p38 nor JNK inhibitors (**Fig.4E and F,** respectively) abrogated the suppression of the IL-4 -induced Arg1 mRNA expression. Interestingly, the rocaglate effect mimicked the effect of the ERK inhibitor U0126 (**Fig.4F**). This was further confirmed by showing that rocaglate suppress ERK1/2 phosphorylation without effecting the levels of total ERK1/2 (**Fig.4G**). This finding is consistent with the previously described role of ERK1/2 in the alternative macrophage activation. (It remains to be determined whether rocaglates inhibit ERK activation directly, or block upstream activators of ERK). One of the relevant downstream targets could be Myc, which transcription is activated by ERK, and whose translation was shown to be selectively inhibited by rocaglates in T cells (*40*). Indeed, Myc activity is necessary for the M2-like macrophage polarization (*41, 42*). Perhaps, in primary macrophages inhibition of the alternative macrophage activation and growth factor responses, reflect physiological response of macrophages to stress that is mimicked by selective inhibition of protein translation.

Potential therapeutic effects of rocaglates

The SQSTM1/p62 protein, which is induced by rocaglates in an IFNγ-independent manner, coordinates activation of central stress response pathways: antioxidative defense and autophagy (*24, 25, 28-33, 43*). Upon oxidative stress, p62 targets KEAP1 protein, an inhibitor of

a transcription factor NRF2, for degradation. NRF2 induces the expression of major anti-oxidant genes. We found that several anti-oxidative genes including catalase, TXNIP and HO-1 were upregulated in macrophages treated with 100 nM of CMLD010536 (**Fig 5A**). Similar to the induction of p62, this effect was also mediated by p38 MAPK (**Fig.5B**). However, ROS were not required for the induction of either p62 or TXNIP by rocaglates, since in both cases ROS scavenger NAC did not reduce their mRNA induction by CMLD010536 (**Fig.2G and Supplemental Fig.3**). Thus, rocaglates can induce upregulation of anti-oxidative defense genes bypassing detrimental ROS generation. To test whether this induction of anti-oxidative pathway provides macrophage protection against subsequent oxidative stress, we challenged macrophages with sodium arsenate, a standard method to induce oxidative stress in vitro. Macrophages pretreated with 30 – 100 nM of CMLD010536 for 6 h survived the exposure to toxic concentration of sodium arsenate, as determined by measuring the percentage of dead (PI positive) macrophages after the 18 h exposure (**Fig. 5C**)**.**

The SQSTM/p62 protein is also a major adaptor protein that mediates selective autophagy and targets intracellular bacteria to LC3-positive autophagosomes(*44*). In addition to the p62 induction, we have previously reported that the rocaglate treatment stimulates autophagic flux and increases the lipidated form of LC3 associated with autophagosome maturation (*16*). Therefore, we tested whether rocaglate pretreatment increased autophagy of intracellular bacteria. BMDM pretreated with CMLD010536 (25 nM) were infected with *Mycobacterium bovis* BCG expressing fluorescent marker GFP (BCG:gfp). At 1, 24 and 48 h post infection (p.i.) macrophages were stained with Lysotracker to access the delivery of the invading bacteria to lysosomes. We observed that pretreatment with the low concentration of CMLD010536 (25 nM) significantly increased the BCG:gfp colocalization with lysosome at 24 and 48 h (**Fig.5D** and **Supplemental Figure 4**). Also, pretreatment with 50 nM CMLD010536 significantly reduced mycobacterial viability, as determined by CFU plating 24 h p.i.(**Fig.5E**). These data demonstrate that priming with the rocaglate significantly increased clearance of a

vacuolar intracellular bacteria (BCG) by macrophages via autophagy induction.

To begin testing effects of rocaglates in vivo, we have chosen a model of acute respiratory challenge with *Streptococcus pneumoniae* (serotype 3). Alveolar macrophages (AM) play an important role at the early phase of this infection (*45, 46*). It is also worth noting that in naïve hosts the AM displays an M2-like phenotype. We wondered whether rocaglate pretreatment could prime macrophages for more efficient control of the acute bacterial infection. Outbred CD-1 IGS male mice were treated with CMLD010536 (25 g/kg, i.p.) at 48, 24 and 0 hours before the respiratory challenge with *Strep. pneumoniae*. At 24 h p.i., bronchoalveolar lavage (BAL) was performed to harvest 2 ml of BAL fluid. We observed significant reduction of live bacteria (as determined by BAL CFU counts, **Fig.5F**, left panel) and BAL cell numbers (**Fig.5F**, right panel) in rocaglate pretreated mice as compared to vehicle-treated controls. These results show that rocaglate pretreatment increased bacterial control and reduced inflammatory cell recruitment to the lungs at the early stage of respiratory infection with *Strep. pneumoniae*.

Discussion

Taken together, our data demonstrate that rocaglates mimic pleiotropic effects of IFNγ on primary macrophages. These effects are dependent on their translation inhibition activity and are mediated by the activation of p38 MAPK and integrated stress response modules. In contrast, the alternative macrophage activation and growth factor responses mediated by STAT6 and ERK are suppressed. Thus, exposure of primary macrophage to rocaglates channels their differentiation toward the M1-like phenotype, boosts their stress resilience and increases control of intracellular bacteria. It is also noteworthy that biological outcomes of rocaglates on primary macrophages are distinct from their better studied effects on tumor cells. Our findings highlight that translational inhibition is necessary but not sufficient to potentiate the rocaglate effect in macrophages, since the general translational inhibitor cycloheximide fails to activate macrophages. In primary macrophages, rocaglate treatment did not block translation completely. Rather, partial shutdown of translation led to reprogramming the macrophage proteome, such that proteins involved in M1-like macrophage activation and stress resilience were upregulated.

Mechanistically, the synthetic and natural rocaglamide derivatives have been shown to inhibit translation by binding to a component of the eIF4F translation initiation complex – the RNA helicase eIF4A – that prevents its incorporation into the eIF4F complex (*47*). However, not all protein translation is equally sensitive to the inhibition of the eIF4A helicase activity. Translation of mRNA species containing structural barriers, such as stem- loop structures or protein–RNA complexes, within their mRNA 5' UTR is most sensitive to eIF4A inhibition. Among the most eIF4A-dependent and rocaglate- sensitive transcripts in acute lymphoblastic leukemia cells were oncogene-encoding transcripts and superenhancer-associated transcription factors, such as Myc (*40*). Because various stressors converge on a common

pathway known as Integrated Stress Response (ISR) leading to inhibition of cap-dependent protein translation, we hypothesize that the eIF4A-mediated selective downregulation of protein translation enables rapid adjustment of the anabolic pathways at translational level to match environmental inputs. Therefore, small molecules that downregulate the eIF4A RNA helicase activity may mimic those stress signals causing adaptive proteome remodeling.

We found that rocaglates potently inhibit ERK phosphorylation, a key activation step in the growth factor signal transduction relay. Phosphorylated ERK promotes cell proliferation and provides anabolic and pro-survival signals primarily via phosphorylation of transcription factors Myc and CREB. Because Myc is known to be critically important for the induction and maintenance of the “trophic” M2-like macrophage state(*41, 42*), ERK inhibition is likely to downregulate the Myc-dependent pathways involved in M2 polarization. According to the literature, ERK can also directly phosphorylate STAT6 and increase its DNA binding and transcriptional activities (*48*). We also observed that rocaglates inhibited IL-4-induced STAT6 DNA binding. Thus, profound inhibition of ERK phosphorylation by rocaglates may explain or significantly contribute to both the STAT6- and Myc-dependent pathways of the M2 polarization and, thus, suppress both the induction and maintenance of the M2-like macrophage phenotype.

The canonical eIF4A-dependent translation inhibition by rocaglates may provide an unknown “stress-like” signal that leads to the inhibition of ERK phosphorylation and, thus, to the coordinated downregulation of several anabolic pathways. Yet, another mechanism may be associated with a recently described alternative target of rocaglates – prohibitin. Rocaglates have been shown to bind prohibitins directly and prevent their interaction with c-Raf, thereby, inhibiting Raf activation and Raf-MEK-ERK signaling in Jurkat tumor cell line. (*22*).
This pathway may lead to translation inhibition by rocaglates via an eIF4A-independent, but ERK-dependent, pathway, since MEK-ERK signaling has been shown to promote cap-dependent translation via phosphorylation of eIF4E, the key translation initiation factor(*22*).

Whether the rocaglate binding to prohibitin mediates ERK inhibition and/or translation inhibition in macrophages remains to be established (*49*)

We demonstrate that rocaglates do not independently initiate the main IFNγ receptor-mediated pathway via STAT1 activation. Instead, they boost effects of IFNγ at concentrations as low as 0.05 -0.2 U/ml. Perhaps, low doses of IFNγ are necessary to provide the canonical Q701 STAT1 phosphorylation by JAK kinases at the IFNγ receptor, which is further amplified by rocaglates. This effect cannot be linked to STAT6 inhibition by rocalates, because a specific STAT6 inhibitor does not recapitulate this effect (**Fig.4H**). Rather, rocaglates induce a synergistic signal via p38 MAPK activation leading to additional STAT1 phosphorylation at Ser 727 (**Fig.3**). This synergy mediates the upregulation of IRF1 mRNA expression. Obviously, the IRF1 protein translation is unimpeded by the rocaglates and, therefore, this central transcription factor in IFNγ network is significantly upregulated. Taken together, our data demonstrate that biological effects of rocaglates on primary macrophage activation are mechanistically linked to translation inhibition and mediated via modulation of MAPK signaling cascades – induction of pro-inflammatory and stress responses by p38 and suppression of anabolic pathways mediated by ERK. Likely, those MAP kinases modulate IFNγ and IL-4 cytokine signaling via STAT1 and STAT6 modifications, respectively.

The biological effects of the rocaglate treatment are not limited to IRF1 induction. They significantly overlap with pleiotropic effects of IFNγ on macrophages, including translation inhibition, autophagy induction and IL-4 suppression (**Supplemental Table 3**). Importantly, rocaglates mimic yet another, less studied, effect of IFNγ. The anti-inflammatory property of IFNγ has been documented in animal models of chronic inflammation, such as streptococcal cell-wall-induced arthritis (*50, 51*), lupus nephritis (*52*) and insulin-dependent diabetes mellitus (*53*). Beneficial effects of IFNγ have also been observed in a rheumatoid arthritis clinical trial (*54*). In a mouse TB model, IFNγ was also shown to limit inflammation and neutrophil influx in the lung, independently of activating the antibacterial activity of macrophages (*55*).

Among known mechanisms by which IFNγ might exert anti-inflammatory responses is induction of cytokine antagonists or decoy receptors, IL-1Ra and IL-18BP (*56-61*). However, the IFN-induced production of IL-1Ra was shown to compromise anti-tuberculous immunity in a mouse model of human-like pulmonary TB. In contrast, an anti-inflammatory activity of rocaglates may be linked to activation of autophagy and anti-oxidant stress response pathways (*24, 62*). Thus, the anti-inflammatory activity of rocaglates can be explained by the active induction of stress resilience mechanisms, rather than by dampening the effector mechanisms of innate immunity. This rocaglate effect can induce pre-programming of monocytes and macrophages to increase their stress resilience prior to encountering potent stressors, deactivating cytokines and virulent pathogens. The exposure to low, subthreshold, doses of stress was shown to prevent subsequent damage by higher doses of stressors in many biological systems. This phenomenon has been termed “hormesis” (*63*) or preconditioning. In this conceptual framework, the anti-inflammatory effect of rocaglates in may be viewed as anticipatory cross-protection, because they dramatically increase the oxidative stress resilience of macrophages via ROS-independent mechanism.

The dissection of signal transduction pathways activated by rocaglates demonstrate that most of their biological effects are achieved via regulatory pathways distinct from those activated by standard concentrations of IFNγ and can be interferon-independent. Therefore, rocaglates may bypass apical signal transduction initiated by the IFNγ binding to the IFNγ receptor. This property of rocaglates may be particularly important for directing macrophage polarization, when the receptor signaling may be disrupted by mutations, microbial factors or negative biological regulators. Thus, rocaglates can be used to guide monocyte/macrophages towards M1-like phenotype and inhibit triggers of the alternative, M2-like, activation in vivo, where the cells are exposed to complex, often conflicting environmental signals(**Fig.6**).

Channeling macrophage differentiation towards the M1-like phenotype would be especially useful in case of co-infections that cause opposite macrophage polarization

programs. For example, by inducing the M2 macrophage polarization, helminth infections may increase susceptibility to mycobacterial infections. Those infections co-exist in endemic regions, such as sub-Saharan Africa and are presumed to contribute to failures of TB vaccination to protect against TB (*6*). Rocaglates may also substitute for decreased production of IFNγ by T cells in HIV-TB co-infections.

We envision that rocaglates may be also useful in chronic non-infectious inflammatory pathologies, where unresolving inflammation is associated with the alternative macrophage activation, such as allergic hypersensitivity in asthma and immune suppression by tumors-associated macrophages. In solid tumors, myeloid cells play a major role in shaping tumor microenvironments (*64, 65*). Tumor associated macrophages (TAM) were implicating in stimulating tumor cell proliferation, angiogenesis, metastasis and resistance to therapy. Those properties have been associated with M2-like differentiation of monocytes guided by cytokines within tumor microenvironments (*66*). In the spatial context of solid tumors, rocaglates may target both the tumor cells decreasing their proliferation and the cells that comprise the immune and inflammatory milieu. The later effects would encompass i) facilitating antigen presentation and T cell priming via induction of autophagy and MHC expression (*67, 68*); ii) blocking M2-like macrophage polarization, and, possibly, iii) prevention of immune suppression also associated with M2-like TAMs and myeloid-derived suppressor cells.

In asthma, allergic reactions may be associated with chronic bacterial infections. Currently, asthma therapy relies on immune suppression by corticosteroids. However, prolonged treatment with steroids may lead to chronic pulmonary infections caused by opportunistic mycobacteria and fungi that further exacerbate pulmonary pathology(*69*)). The important theoretical advantage of rocaglates as compared to corticosteroids, is that rocaglates would shift the balance of macrophage activation towards M1-like phenotype and not suppress mechanisms of macrophage resistance to infections.

448

Figure legends

Figure 1. Translation inhibition is required for rocaglate to activate BMDM.

A) Twenty three rocaglate analogues were examined for their translation inhibition activity and induction of IRF1 gene expression with 0.3 μM at 24 h in presence of a low dose of IFNγ (0.1U/ml). The correlation coefficient was calculated in GraphPad Prism.

B) Chemical structure of CMLD010536 and CMLD010850.

C) BMDM was treated with indicated concentration (μM) of CMLD010536 and CMLD010850 for 2 h followed by 1 h treatment with 5 ug/ml puromycin. Puromycin incorporation was monitored by western blot using puromycin-specific antibody.

D) BMDMs were treated with 100 nM CMLD010536 (labeled as 536) and CMLD010850 (labeled as 850). IRF1 and TXNIP gene expression was compared using qRT-PCR.

Figure 2. Selective translation inhibition by rocaglate leads to altered macrophage proteome.

A) BMDM was treated with 0.1 and 0.3 μM CMLD010536 for 2, 8 and 23 h followed by a treatment with 5 μg/ml puromycin for additional 1 h. Incorporation of puromycin was monitored by Western blot using puromycin-specific antibody.

B) Macrophages were treated with 25, 50 and 100 nM CMLD010536 for 6 and 24 h. Expression of p62 protein was measured by Western blot by p62-specific antibody. Untreated cells were used as a control.

C) Mouse macrophages were treated with 25, 50 and 100 nM CMLD010536 for 6 h and induction of p62 mRNA compared to untreated cells was measured by real-time PCR.

D) Macrophages were pretreated with 10 μM p38 (SB203580), JNK (SB600125), and ERK (U0126) inhibitor(s) for 30 min followed by treatment with 100 nM CMLD010536 for additional 6 h. p62 mRNA expression was measured by real-time PCR.

E) Macrophages were treated with 0.3 μM CMLD010536 for the indicated amount of time and the activation of the p-38 pathway was evidenced by Western blot using phospho-p38 specific antibody.

F) Macrophages were treated with 100 nM CMLD010536 for the indicated amount of time and induction of p62 mRNA was measured by real time PCR.

G) Macrophages were pretreated with 40 nM NAC for 1 h followed by treatment with 100 nM CMLD010536 for another 6 h, and p62 mRNA expression was compared against macrophages treated with 100 nM CMLD010536 alone. NAC-only treated cells were run as control.

H) Macrophages were treated with 100 nM CMLD010536 (536), sivestrol (sil), rocaglamide A (RocA) and CMLD010850 for 24 h and induction of p62 mRNA was measured by real time PCR compare to untreated cells.

I) Macrophages were treated with 100 and 300 nM CMLD010536, rapamycin and cycloheximide for 6 h and induction of p62 mRNA was measured by real time PCR compare to untreated cell.

J and K) BMDM was treated with 100 nM CMLD010536 for the indicated time and the ATF3 mRNA (J) and protein (K) levels were measured by qRT-PVR and Western blot, respectively.

Figure 3. Stress kinase activation by rocaglates

A) Macrophages were pretreated with 10 μM p38 inhibitor (SB203580) for 30 min followed by treatment with 0.3 μM CMLD010536 and 0.05 or 0.1 U/ml IFNγ for 6 h. IRF1 protein expression was measured by Western blot using IRF1-specific antibody. Relative densitometric values are shown above

B) Macrophages were treated with 0.3 μM CMLD010536 either in the absence or in the presence of 0.1 U/ml IFNγ for indicated periods of time and activation of the p-38 pathway was evidenced by Western blot using phospho-p38 specific antibody.

C) Macrophages were pretreated with 10 μM of MAPK-p38 inhibitor (SB203580), JNK inhibitor (SB600125) and ERK inhibitor (U0126) for 30 min followed by treatment with 0.3 μM CMLD010536 and 0.2 U/ml IFNγ for additional 4 h. The IRF1 mRNA expression was measured by qRT-PCR.

D) Macrophages were treated with 0.2, 2 and 20 U/ml IFNγ for 4 h either with the pretreatment with 10 μM p38 inhibitor SB203580 for 30 min, or no pretreatment. IRF1 mRNA expression in macrophages was measured by qRT-PCR.

E) Macrophages were treated with 0.3 μM CMLD010536 for indicated amount of time and phosphorylation of STAT1 at Ser727 was monitored by Western blot using phospho-Ser727-specific antibody.

Figure 4. Suppression of alternate activation of macrophages by rocaglates.

A) Primary bone marrow derived macrophages were pretreated with either indicated concentrations of IFNγ or CMLD010536 for 4 h, followed by a treatment with 25 ng/ml IL4 for additional 20 h. Suppression of Arg1 mRNA was measured using qRT-PCR.

B) Suppression of STAT6 promoter binding activity was monitored by gel mobility shift experiment. Macrophages were pretreated with indicated concentration of CMLD010536 for 2 h followed by a treatment with IL4 (25 ng/ml) for additional 4 h. Nuclear extract was prepared and STAT6 promoter binding activity was monitored by EMSA using STAT6 specific DNA probe. A cold competition control was run for both cases to show the specificity of the shifted band.

C) Total cellular and nuclear STAT6 protein level was measured by Western blot. Macrophages were treated with indicated concentration of CMLD010536 for 2 h followed by a treatment with IL4 (25 ng/ml) for additional 4 h. STAT6 level was compared with IL4 only treated control.

D) Suppression of IL4-induced Arg1 gene expression was compared for 100 nM CMLD010536, CMLD010850, silvestrol and rocaglamide A. BMDMs were pretreated with rocaglate derivatives for 4 h followed by a treatment with 25 ng/ml of IL4 for additional 20 h.

E) BMDMs were treated with 10 μM p38 inhibitor SB203580 for 30 mins followed by CMLD010536 (100 nM) and IL-4 (25 ng/ml). Expression of arginase I mRNA was measured using qRT-PCR.

F) BMDMs were treated with JNK or ERK inhibitors or CMLD010536 for 30 mins followed by IL-4 (25 ng/ml). Expression of arginase I mRNA was measured using qRT-PCR.

G) BMDMs were pre-treated with 100 nM CMLD010536 for 12 h followed by treatment with 100 ng/ml IL4 for the indicated periods of time. Phospho-ERK1/2 and total ERK1/2 amounts were measured by Western blot.

H) BMDMs were treated with either 10, 30 or 100 nM CMLD010536 or STAT6 inhibitor AS1517499 in increasing doses in the presence of 0.2 U/ml IFNγ. IRF1 mRNA expression was measured using qRT-PCR.

Figure 5. Biological effects of rocaglates: induction of anti-oxidant and antibacterial defenses

A) Primary macrophages were treated with 100 nM of CMLD010536 for 24 h and mRNA expression for Catalase, TXNIP, NQo-1 and HO-1 were measured by real-time PCR.

B) Macrophages were pretreated with kinase inhibitor 10 μM p38 (SB203580), JNK (SB600125), and ERK (U0126) for 30 min followed by a treatment with 100 nM CMLD010536 for additional 24 h. mRNA expression for TXNIP, was measured by real-time PCR.

C) Macrophages were pretreated with 30 nM CMLD010536 for 2 h followed a challenge with 5 uM with Sodium arsenate (Ar) for additional 16 h. Cytotoxicity was measured as % of PI positive cells using automated microscopy.

D) BMDMs were pretreated with CMLD010536 (50 nM) for 6 h and infected with *M.bovis* BCG:gfp at MOI:1. Cells were stained with Lysotracker at 1, 24 and 48 h post infection.

E) BMDMs were treated with CMLD010536 and infected 24 hours later with of BCG (MOI 1, 3). The BCG loads were enumerated by CFU plating.

F) CD-1 IGS outbred male mice were injected i.p. with CMLD010536 (25 mcg/kg) or the vehicle control at 48, 24 and 0 h before respiratory infection with *Strep.pneumoniae*. At 24 h p.i., BAL fluid was harvested to determine viable bacterial counts (CFU, left panel) and total BAL cells (right panel).

Figure 6. Summary of rocaglate activities in primary macrophages

Materials and Methods

Mice

C57BL/6 J mice were obtained from the Jackson Laboratory (Bar Harbor, Maine, USA). All experiments were performed with the full knowledge and approval of the Standing Committee on Animals at Boston University in accordance with relevant guidelines and regulations (IACUC protocol number AN15276).

BMDM culture

Isolation of mouse bone marrow and culture of BMDMs were carried out as previously described (Pan H. 2008). Mouse macrophages were cultured in DMEM/F12 containing 10% fetal bovine serum supplemented with 1% glutamine, penicillin and streptomycin (100 U/mL and 100 μg/mL respectively) and 10 mM Hepes buffer (complete medium).

Gel shift assay

The nuclear extracts were prepared by Signosis Inc. nuclear extraction kits. Gel shift assays were done with EMSA kits (Signosis Inc). 5 μg nuclear extracts were incubated with 1× binding buffer and biotin-labeled probe for 30 min at room temperature to form protein/DNA complexes. The samples were then electrophoresed on a 6 % polyacrylamide gel in 0.5 % TBE at 120 V for 45 min and then transferred onto a nylon membrane in 0.5 % TBE at 300 mA for 1 h. After transfer and UV cross-linking, the membrane was detected with Streptavidin–HRP.

Immunoblotting

BMDMs were subjected to treatments specified in the text. Whole cell extracts were prepared by lysing the cells in RIPA buffer supplemented with protease inhibitor cocktail and phosphatase inhibitor I and II (Sigma). Equal amounts (50 μg) of protein from whole-cell extracts was separated by SDS-PAGE and transferred to PVDF membrane (Millipore). After blocking with 5% skim milk in TBS-T buffer [20 mM Tris–HCl (pH 7.5), 150 mM NaCl, and

0.1% Tween20] for 2 hour, the membranes were incubated with the primary antibody overnight at 4 °C. Bands were detected with enhanced chemiluminescence (ECL) kit (Perkin Elmer). Stripping was performed using WB stripping solution (Thermo scientific). The loading control β-actin (Sigma, 1:10000) was evaluated on the same membrane. IRF1 antibody was obtained from Cell Signaling (1:500). Phospho-p38 antibodies were obtained from Cell signaling (1:250). STAT1 (Ser 727) and STAT6 were obtained from Abcam. Fold induction of the proteins were calculated relative to untreated (set as 1) by densitometric analysis after normalizing it to loading control β-actin.

RNA isolation and quantitative PCR

Total RNA was isolated using the RNeasy Plus mini kit (Qiagen). cDNA synthesis was performed using the SuperScript II (Invitrogen). Real-time PCR was performed with the GoTaq qPCR Mastermix (Promega) using the CFX-90 real-time PCR System (Bio-Rad). Thermal cycling parameters involved 40 cycles under the following conditions: 95 °C for 2 min, 95 °C for 15 s and 60 °C for 30 s. Each sample was set up in triplicate and normalized to RPS17 or 18 S expression by the DDCt method.

Hoechst/PI staining method for cell cytotoxicity

For cell viability assays BMDMs were plated in 96 well tissue culture plates (12000 cells/well) and subjected to necessary treatments. The supernatant was aspirated and to each well 100 µl PBS containing Hoechst (Invitrogen, 10 µM) and PI (Calbiochem, 2 µM) were added. The plates were kept at 37 °C for 15 min and read in an automated cell cytometer. The % of total and dead cells was calculated for each treatment.

Reporter assay for measuring translation inhibition

293TR-FLuc cells that stably express Renilla firefly luciferase were grown in complete medium and were a gift from Luke Whitesell of the Whitehead Institute. 293TR-Fluc cells were grown to confluence and maintained in complete medium. 10,000 cells were plated in a 96-well clear bottom plate in complete medium without phenol-red. Compounds were added

at different dilutions and kept for 18 h. The next day the media was removed and 100 ul of Nanolight Firefly Luc Assay reagent was added to the wells and the luminescence was measured using a Tecan-plate reader after 2 mins. Cells treated with DMSO served as negative controls and with 100 µg/mL cycloheximide served as positive controls. Percentage of translation inhibition for each compound was calculated in triplicates from two independent experiments.

Puromycin incorporation assay

Puromycin labelling for measuring the intensity of translation was performed as previously described(*70*). For immunoblots, 5 µg/ml puromycin (Sigma, min 98% TLC, cell culture tested, P8833, diluted in PBS) was added in the culture medium and the cells were incubated for 1 h at 37 °C and 5% CO_2. Cells were washed with cold PBS prior to cell lysis, centrifuged at 4 °C and immunoblotting was performed with the anti-puromycin antibody clone12D10 (1:10000) (Millipore).

Phagosome–lysosome fusion assay

The murine bone marrow derived macrophages were cultured in DMEM F12 medium (composition), supplemented with 10 % heat inactivated fetal calf serum and LCCM at 37 °C and 5 % CO_2. The cells were pretreated with CMLD010536 (25 nM) for 6 h and subsequently infected with log-phase culture of *M. bovis* BCG expressing *gfp* (BCG:*gfp*) for 1 h at MOI 1. To remove the extracellular bacteria the cells were treated with 200 ug/ml of amikacin for 1 h. After 1 h, 24 h and 48 h post-infection, cells were stained with 200 nM of LysoTracker red dye for 1 h at 37 °C. Cells were then fixed in 4% para-formaldehyde for 10 min. After every step mentioned above the cells were washed 2 times with PBS. The stained cells were mounted, kept overnight at room temperature and analyzed using Zeiss LSM 710-Live Duo scan confocal microscope. The images were processed using FIJI software and the percentage of co-localization of BCG:*gfp* containing phagosomes with LysoTracker red dye was calculated by dividing the number of co-localized phagosomes by the total number of phagosomes. At least 50 cells are

measured at each condition and the mean ± SEM (*p value* was >0.05) was calculated using GraphPad Prism.

Bacterial CFU:

BMDM were grown in 96 well tissue culture plate and infected with BCG. Bacterial load at each condition was determined by standard CFU plating. To be specific, media was removed from wells, washed 3 times with 1 x PBS containing 1% FCS and lysed with 50 ul of 1% Triton-X100 by incubating for 10 min at room temp. Lysate was plated on 7H10 agar plate supplemented with 10% oleic acid-albumin-dextrose-catalase in triplicate for each condition after serial dilution. Colonies were counted after incubation of the plates at 37 °C for 3 weeks.

Acknowledgments

This work was supported by the National Institutes of Health, award numbers R33 AI105944-04 and R01 HL133190-01 (IK), 1R01GM120272 (ARI) and R01CA218500 (ARI). The authors are grateful to Dr. John Connor for helpful discussions.

The authors declare no competing interests.

References:

1. R. S. Wallis, R. Hafner, Advancing host-directed therapy for tuberculosis. *Nat Rev Immunol* **15**, 255-263 (2015).
2. L. Heitmann *et al.*, The IL-13/IL-4Ralpha axis is involved in tuberculosis-associated pathology. *J Pathol* **234**, 338-350 (2014).
3. T. Chanmee, P. Ontong, K. Konno, N. Itano, Tumor-associated macrophages as major players in the tumor microenvironment. *Cancers (Basel)* **6**, 1670-1690 (2014).
4. A. Sica, A. Mantovani, Macrophage plasticity and polarization: in vivo veritas. *J Clin Invest* **122**, 787-795 (2012).
5. J. A. Potian *et al.*, Preexisting helminth infection induces inhibition of innate pulmonary anti-tuberculosis defense by engaging the IL-4 receptor pathway. *J Exp Med* **208**, 1863-1874 (2011).
6. P. Salgame, G. S. Yap, W. C. Gause, Effect of helminth-induced immunity on infections with microbial pathogens. *Nat Immunol* **14**, 1118-1126 (2013).
7. J. Harris *et al.*, T helper 2 cytokines inhibit autophagic control of intracellular Mycobacterium tuberculosis. *Immunity* **27**, 505-517 (2007).
8. S. Y. Patel *et al.*, Anti-IFN-gamma autoantibodies in disseminated nontuberculous mycobacterial infections. *J Immunol* **175**, 4769-4776 (2005).
9. S. K. Browne, S. M. Holland, Anticytokine autoantibodies in infectious diseases: pathogenesis and mechanisms. *Lancet Infect Dis* **10**, 875-885 (2010).
10. C. Venkataraman, S. Leung, A. Salvekar, H. Mano, U. Schindler, Repression of IL-4-induced gene expression by IFN-gamma requires Stat1 activation. *J Immunol* **162**, 4053-4061 (1999).
11. A. M. Cadena, S. M. Fortune, J. L. Flynn, Heterogeneity in tuberculosis. *Nat Rev Immunol* **17**, 691-702 (2017).
12. B. Carow *et al.*, Spatial and temporal localization of immune transcripts defines hallmarks and diversity in the tuberculosis granuloma. *Nat Commun* **10**, 1823 (2019).
13. S. Marino *et al.*, Macrophage polarization drives granuloma outcome during Mycobacterium tuberculosis infection. *Infect Immun* **83**, 324-338 (2015).
14. S. Sakai, K. D. Mayer-Barber, D. L. Barber, Defining features of protective CD4 T cell responses to Mycobacterium tuberculosis. *Curr Opin Immunol* **29**, 137-142 (2014).
15. J. D. Ernst, Mechanisms of M. tuberculosis Immune Evasion as Challenges to TB Vaccine Design. *Cell Host Microbe* **24**, 34-42 (2018).
16. B. Bhattacharya *et al.*, Fine-tuning of macrophage activation using synthetic rocaglate derivatives. *Sci Rep* **6**, 24409 (2016).
17. S. Santagata *et al.*, Tight coordination of protein translation and HSF1 activation supports the anabolic malignant state. *Science* **341**, 1238303 (2013).
18. B. Y. Hwang *et al.*, Silvestrol and episilvestrol, potential anticancer rocaglate derivatives from Aglaia silvestris. *J Org Chem* **69**, 3350-3358 (2004).
19. S. Kim *et al.*, Silvestrol, a potential anticancer rocaglate derivative from Aglaia foveolata, induces apoptosis in LNCaP cells through the mitochondrial/apoptosome pathway without activation of executioner caspase-3 or -7. *Anticancer Res* **27**, 2175-2183 (2007).

20. S. Kim, A. A. Salim, S. M. Swanson, A. D. Kinghorn, Potential of cyclopenta[b]benzofurans from Aglaia species in cancer chemotherapy. *Anticancer Agents Med Chem* **6**, 319-345 (2006).
21. M. E. Bordeleau *et al.*, Therapeutic suppression of translation initiation modulates chemosensitivity in a mouse lymphoma model. *J Clin Invest* **118**, 2651-2660 (2008).
22. G. Polier *et al.*, The natural anticancer compounds rocaglamides inhibit the Raf-MEK-ERK pathway by targeting prohibitin 1 and 2. *Chem Biol* **19**, 1093-1104 (2012).
23. C. M. Rodrigo, R. Cencic, S. P. Roche, J. Pelletier, J. A. Porco, Synthesis of rocaglamide hydroxamates and related compounds as eukaryotic translation inhibitors: synthetic and biological studies. *J Med Chem* **55**, 558-562 (2012).
24. Y. Katsuragi, Y. Ichimura, M. Komatsu, p62/SQSTM1 functions as a signaling hub and an autophagy adaptor. *FEBS J* **282**, 4672-4678 (2015).
25. J. Moscat, M. T. Diaz-Meco, Feedback on fat: p62-mTORC1-autophagy connections. *Cell* **147**, 724-727 (2011).
26. H. Knaevelsrud, A. Simonsen, Fighting disease by selective autophagy of aggregate-prone proteins. *FEBS Lett* **584**, 2635-2645 (2010).
27. T. Johansen, T. Lamark, Selective autophagy mediated by autophagic adapter proteins. *Autophagy* **7**, 279-296 (2011).
28. K. Taguchi, H. Motohashi, M. Yamamoto, Molecular mechanisms of the Keap1-Nrf2 pathway in stress response and cancer evolution. *Genes Cells* **16**, 123-140 (2011).
29. M. C. Jaramillo, D. D. Zhang, The emerging role of the Nrf2-Keap1 signaling pathway in cancer. *Genes Dev* **27**, 2179-2191 (2013).
30. B. Padmanabhan *et al.*, Structural basis for defects of Keap1 activity provoked by its point mutations in lung cancer. *Mol Cell* **21**, 689-700 (2006).
31. T. Fukutomi, K. Takagi, T. Mizushima, N. Ohuchi, M. Yamamoto, Kinetic, thermodynamic, and structural characterizations of the association between Nrf2-DLGex degron and Keap1. *Mol Cell Biol* **34**, 832-846 (2014).
32. M. Komatsu *et al.*, The selective autophagy substrate p62 activates the stress responsive transcription factor Nrf2 through inactivation of Keap1. *Nat Cell Biol* **12**, 213-223 (2010).
33. A. Lau *et al.*, A noncanonical mechanism of Nrf2 activation by autophagy deficiency: direct interaction between Keap1 and p62. *Mol Cell Biol* **30**, 3275-3285 (2010).
34. M. A. Meraz *et al.*, Targeted disruption of the Stat1 gene in mice reveals unexpected physiologic specificity in the JAK-STAT signaling pathway. *Cell* **84**, 431-442 (1996).
35. T. Decker, P. Kovarik, A. Meinke, GAS elements: a few nucleotides with a major impact on cytokine-induced gene expression. *J Interferon Cytokine Res* **17**, 121-134 (1997).
36. A. C. Dudley, D. Thomas, J. Best, A. Jenkins, The STATs in cell stress-type responses. *Cell Commun Signal* **2**, 8 (2004).
37. Z. Wen, Z. Zhong, J. E. Darnell, Jr., Maximal activation of transcription by Stat1 and Stat3 requires both tyrosine and serine phosphorylation. *Cell* **82**, 241-250 (1995).
38. P. Kovarik, D. Stoiber, M. Novy, T. Decker, Stat1 combines signals derived from IFN-gamma and LPS receptors during macrophage activation. *EMBO J* **17**, 3660-3668 (1998).
39. K. C. Goh, S. J. Haque, B. R. Williams, p38 MAP kinase is required for STAT1 serine phosphorylation and transcriptional activation induced by interferons. *EMBO J* **18**, 5601-5608 (1999).

40. A. L. Wolfe *et al.*, RNA G-quadruplexes cause eIF4A-dependent oncogene translation in cancer. *Nature* **513**, 65-70 (2014).
41. O. M. Pello, Macrophages and c-Myc cross paths. *Oncoimmunology* **5**, e1151991 (2016).
42. O. M. Pello *et al.*, Role of c-MYC in alternative activation of human macrophages and tumor-associated macrophage biology. *Blood* **119**, 411-421 (2012).
43. V. Rogov, V. Dotsch, T. Johansen, V. Kirkin, Interactions between autophagy receptors and ubiquitin-like proteins form the molecular basis for selective autophagy. *Mol Cell* **53**, 167-178 (2014).
44. Y. T. Zheng *et al.*, The adaptor protein p62/SQSTM1 targets invading bacteria to the autophagy pathway. *J Immunol* **183**, 5909-5916 (2009).
45. D. H. Dockrell *et al.*, Alveolar macrophage apoptosis contributes to pneumococcal clearance in a resolving model of pulmonary infection. *J Immunol* **171**, 5380-5388 (2003).
46. S. B. Gordon, G. R. Irving, R. A. Lawson, M. E. Lee, R. C. Read, Intracellular trafficking and killing of Streptococcus pneumoniae by human alveolar macrophages are influenced by opsonins. *Infect Immun* **68**, 2286-2293 (2000).
47. R. Cencic *et al.*, Antitumor activity and mechanism of action of the cyclopenta[b]benzofuran, silvestrol. *PLoS One* **4**, e5223 (2009).
48. E. Y. So, J. Oh, J. Y. Jang, J. H. Kim, C. E. Lee, Ras/Erk pathway positively regulates Jak1/STAT6 activity and IL-4 gene expression in Jurkat T cells. *Mol Immunol* **44**, 3416-3426 (2007).
49. J. Chu, R. Cencic, W. Wang, J. A. Porco, Jr., J. Pelletier, Translation Inhibition by Rocaglates Is Independent of eIF4E Phosphorylation Status. *Mol Cancer Ther* **15**, 136-141 (2016).
50. S. M. Wahl, J. B. Allen, K. Ohura, D. E. Chenoweth, A. R. Hand, IFN-gamma inhibits inflammatory cell recruitment and the evolution of bacterial cell wall-induced arthritis. *J Immunol* **146**, 95-100 (1991).
51. J. B. Allen *et al.*, Suppression of bacterial cell wall-induced polyarthritis by recombinant gamma interferon. *Cytokine* **3**, 98-106 (1991).
52. Double blind controlled phase III multicenter clinical trial with interferon gamma in rheumatoid arthritis. German Lymphokine Study Group. *Rheumatol Int* **12**, 175-185 (1992).
53. F. Nicoletti *et al.*, Paradoxical antidiabetogenic effect of gamma-interferon in DP-BB rats. *Diabetes* **47**, 32-38 (1998).
54. K. P. Machold, K. Neumann, J. S. Smolen, Recombinant human interferon gamma in the treatment of rheumatoid arthritis: double blind placebo controlled study. *Ann Rheum Dis* **51**, 1039-1043 (1992).
55. B. Nandi, S. M. Behar, Regulation of neutrophils by interferon-gamma limits lung inflammation during tuberculosis infection. *J Exp Med* **208**, 2251-2262 (2011).
56. C. A. Dinarello, Biologic basis for interleukin-1 in disease. *Blood* **87**, 2095-2147 (1996).
57. W. P. Arend, M. Malyak, C. J. Guthridge, C. Gabay, Interleukin-1 receptor antagonist: role in biology. *Annu Rev Immunol* **16**, 27-55 (1998).
58. D. Novick *et al.*, Interleukin-18 binding protein: a novel modulator of the Th1 cytokine response. *Immunity* **10**, 127-136 (1999).
59. Y. Aizawa *et al.*, Cloning and expression of interleukin-18 binding protein. *FEBS Lett* **445**, 338-342 (1999).

60. S. H. Kim *et al.*, Structural requirements of six naturally occurring isoforms of the IL-18 binding protein to inhibit IL-18. *Proc Natl Acad Sci U S A* **97**, 1190-1195 (2000).
61. C. A. Dinarello, Targeting interleukin 18 with interleukin 18 binding protein. *Ann Rheum Dis* **59 Suppl 1**, i17-20 (2000).
62. Y. Du, M. C. Wooten, M. Gearing, M. W. Wooten, Age-associated oxidative damage to the p62 promoter: implications for Alzheimer disease. *Free Radic Biol Med* **46**, 492-501 (2009).
63. E. J. Calabrese, Hormesis: why it is important to toxicology and toxicologists. *Environ Toxicol Chem* **27**, 1451-1474 (2008).
64. M. C. Schmid, J. A. Varner, Myeloid cells in the tumor microenvironment: modulation of tumor angiogenesis and tumor inflammation. *J Oncol* **2010**, 201026 (2010).
65. P. J. Murray, Nonresolving macrophage-mediated inflammation in malignancy. *FEBS J* **285**, 641-653 (2018).
66. S. I. Grivennikov, F. R. Greten, M. Karin, Immunity, inflammation, and cancer. *Cell* **140**, 883-899 (2010).
67. V. L. Crotzer, J. S. Blum, Autophagy and its role in MHC-mediated antigen presentation. *J Immunol* **182**, 3335-3341 (2009).
68. C. Munz, Antigen processing via autophagy--not only for MHC class II presentation anymore? *Curr Opin Immunol* **22**, 89-93 (2010).
69. L. G. Fritscher *et al.*, Nontuberculous mycobacterial infection as a cause of difficult-to-control asthma: a case-control study. *Chest* **139**, 23-27 (2011).
70. E. K. Schmidt, G. Clavarino, M. Ceppi, P. Pierre, SUnSET, a nonradioactive method to monitor protein synthesis. *Nat Methods* **6**, 275-277 (2009).

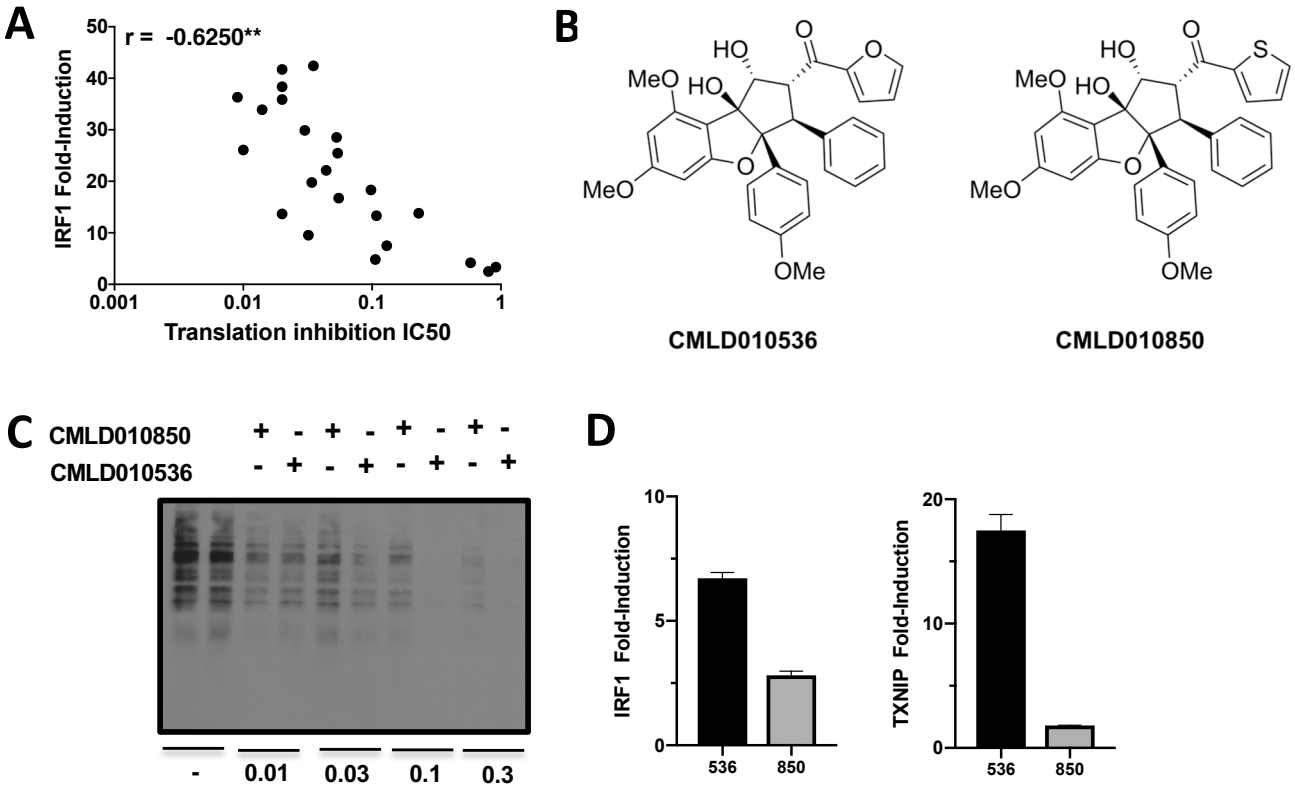
A
r = -0.6250**
IRF1 Fold-Induction
Translation inhibition IC50
B
CMLD010536
CMLD010850
C
CMLD010850
CMLD010536
-
0.01
0.03
0.1
0.3
D
IRF1 Fold-Induction
TXNIP Fold-Induction
536
850

Fig.1

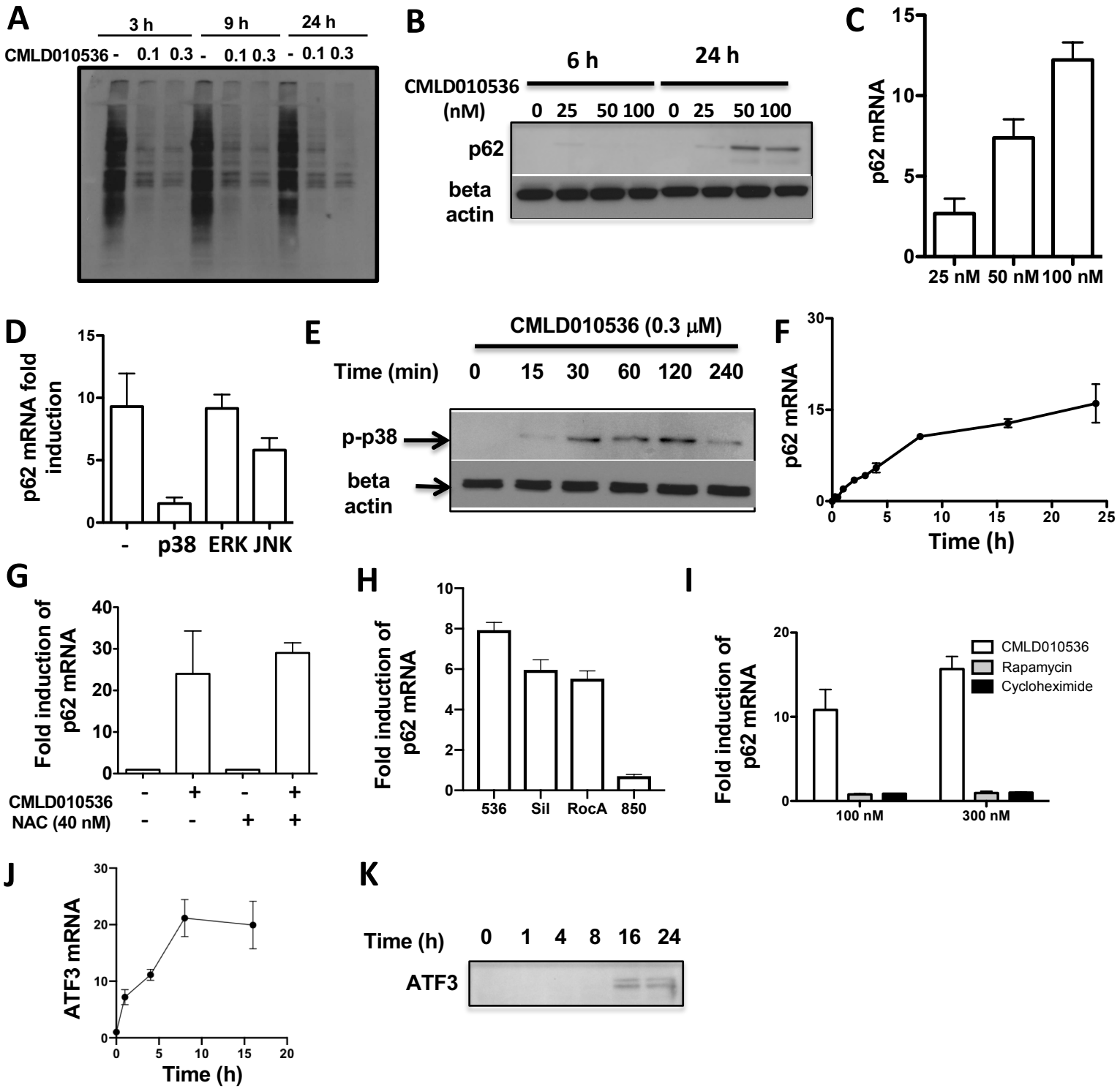
A
3 h
9 h
24 h
CMLD010536 - 0.1 0.3 - 0.1 0.3 - 0.1 0.3
B
6 h
24 h
CMLD010536 (nM)
0 25 50 100 0 25 50 100
p62
beta actin
C
p62 mRNA
25 nM 50 nM 100 nM
D
p62 mRNA fold induction
- p38 ERK JNK
E
CMLD010536 (0.3 μM)
Time (min) 0 15 30 60 120 240
p-p38
beta actin
F
p62 mRNA
Time (h)
G
Fold induction of p62 mRNA
CMLD010536
NAC (40 nM)
H
Fold induction of p62 mRNA
536 Sil RocA 850
I
Fold induction of p62 mRNA
CMLD010536
Rapamycin
Cycloheximide
100 nM 300 nM
J
ATF3 mRNA
Time (h)
K
Time (h) 0 1 4 8 16 24
ATF3

Fig.2

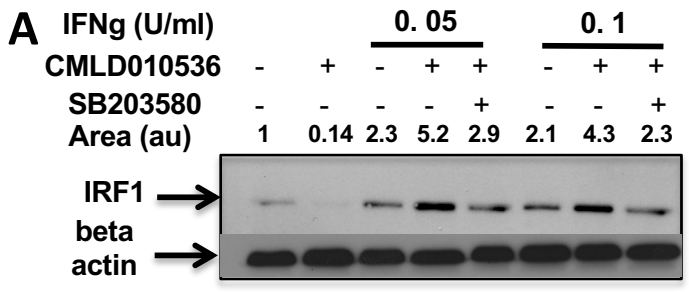
A
IFNg (U/ml)
0. 05
0. 1
CMLD010536 - + - + + - + +
SB203580 - - - - + - - +
Area (au) 1 0.14 2.3 5.2 2.9 2.1 4.3 2.3
IRF1
beta actin

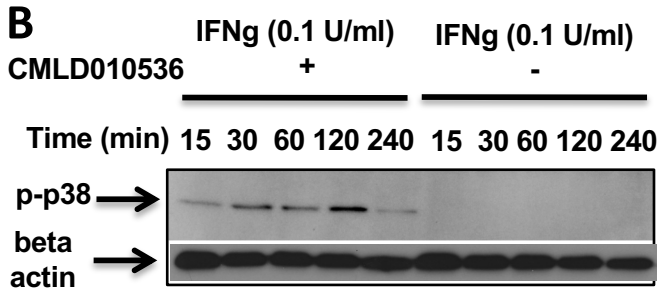
B
IFNg (0.1 U/ml)
IFNg (0.1 U/ml)
CMLD010536 + -
Time (min) 15 30 60 120 240 15 30 60 120 240
p-p38
beta actin

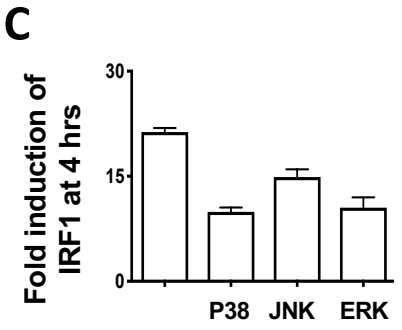
C
Fold induction of IRF1 at 4 hrs
30
15
0
P38
JNK
ERK

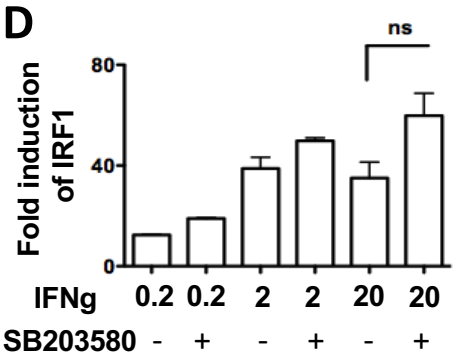
D
ns
Fold induction of IRF1
80
40
0
IFNg 0.2 0.2 2 2 20 20
SB203580 - + - + - +

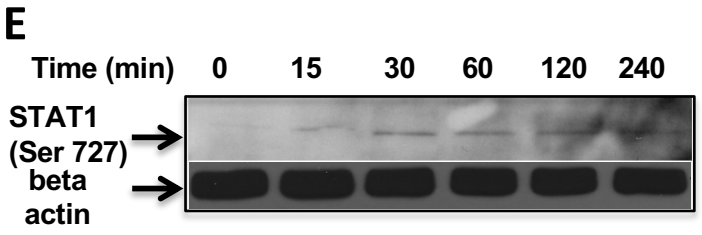
E
Time (min) 0 15 30 60 120 240
STAT1 (Ser 727)
beta actin

Fig.3

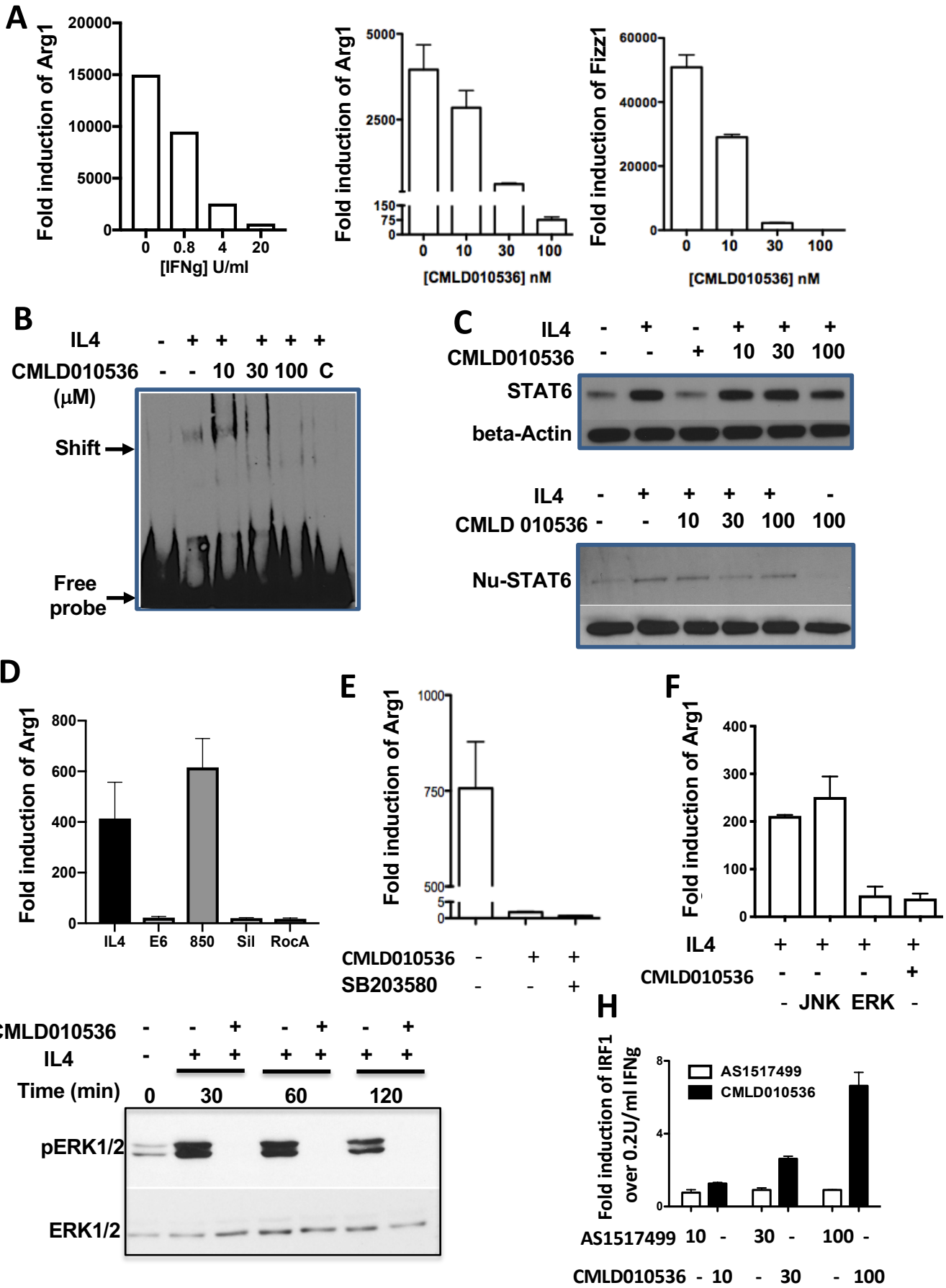
A
Fold induction of Arg1
20000
15000
10000
5000
0
0
0.8
4
20
[IFNg] U/ml
Fold induction of Arg1
5000
2500
150
75
0
0
10
30
100
[CMLD010536] nM
Fold induction of Fizz1
60000
40000
20000
0
0
10
30
100
[CMLD010536] nM
B
IL4 - + + + + +
CMLD010536 (μM) - - 10 30 100 C
Shift
Free probe
C
IL4 - + - + + +
CMLD010536 - - + 10 30 100
STAT6
beta-Actin
IL4 - + + + + -
CMLD 010536 - - 10 30 100 100
Nu-STAT6
D
Fold induction of Arg1
800
600
400
200
0
IL4
E6
850
Sil
RocA
E
Fold induction of Arg1
1000
750
500
5
0
CMLD010536 - + +
SB203580 - - +
F
Fold induction of Arg1
400
300
200
100
0
IL4 + + + +
CMLD010536 - - - +
- JNK ERK -
G
CMLD010536 - - + - + - +
IL4 - + + + + + +
Time (min) 0 30 60 120
pERK1/2
ERK1/2
H
Fold induction of IRF1 over 0.2U/ml IFNg
8
4
0
AS1517499
CMLD010536
AS1517499 10 - 30 - 100 -
CMLD010536 - 10 - 30 - 100

Fig.4

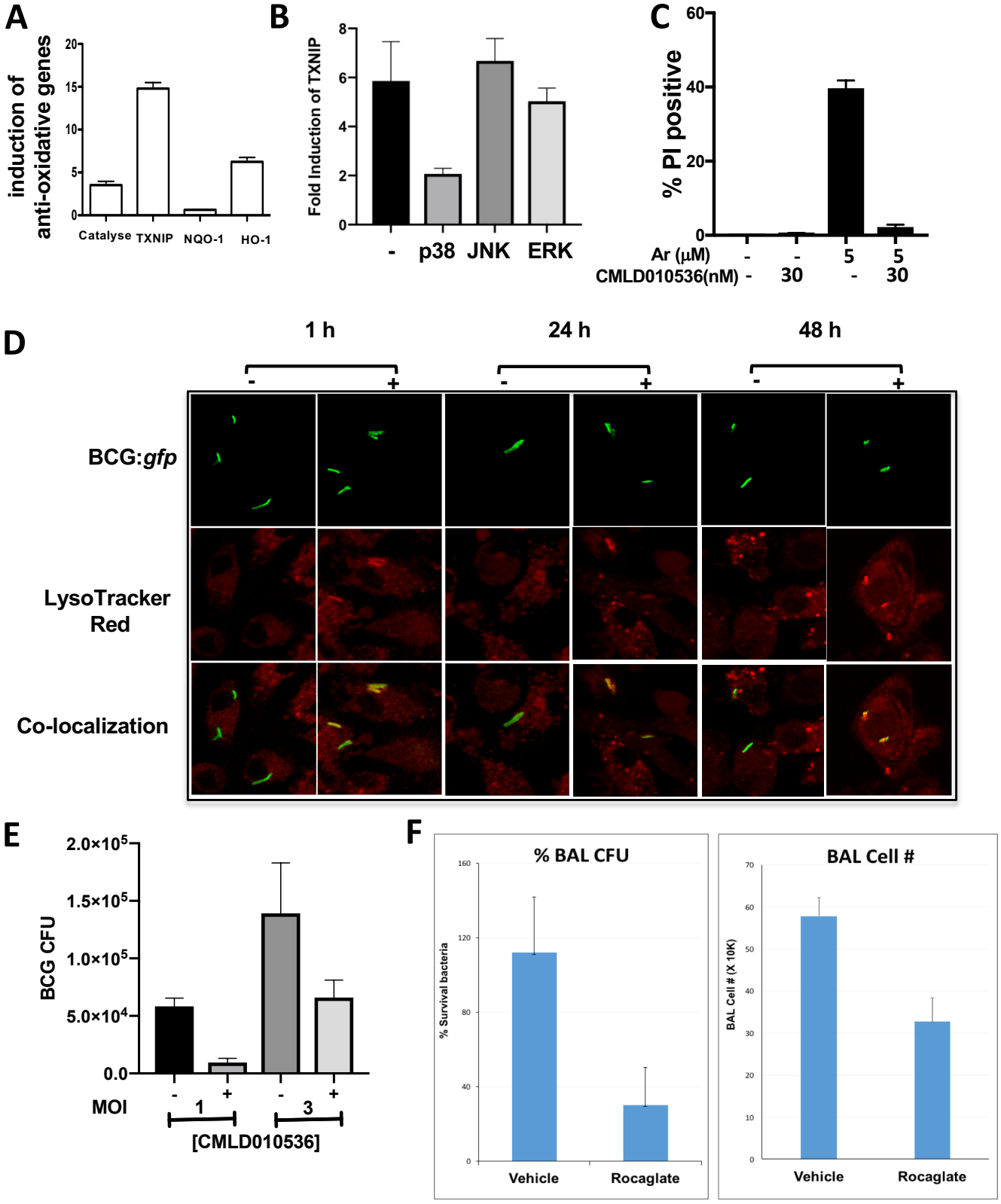
A
induction of anti-oxidative genes
20
15
10
5
0
Catalyse
TXNIP
NQO-1
HO-1
B
Fold Induction of TXNIP
8
6
4
2
0
-
p38
JNK
ERK
C
% PI positive
60
40
20
0
Ar (μM) - - 5 5
CMLD010536(nM) - 30 - 30
D
1 h
24 h
48 h
- + - + - +
BCG:gfp
LysoTracker Red
Co-localization
E
BCG CFU
2.0×10^5
1.5×10^5
1.0×10^5
5.0×10^4
0.0
MOI
- + - +
1
3
[CMLD010536]
F
% BAL CFU
% Survival bacteria
160
120
80
40
0
Vehicle
Rocaglate
BAL Cell #
BAL Cell # (X 10K)
70
60
50
40
30
20
10
0
Vehicle
Rocaglate

Fig 5

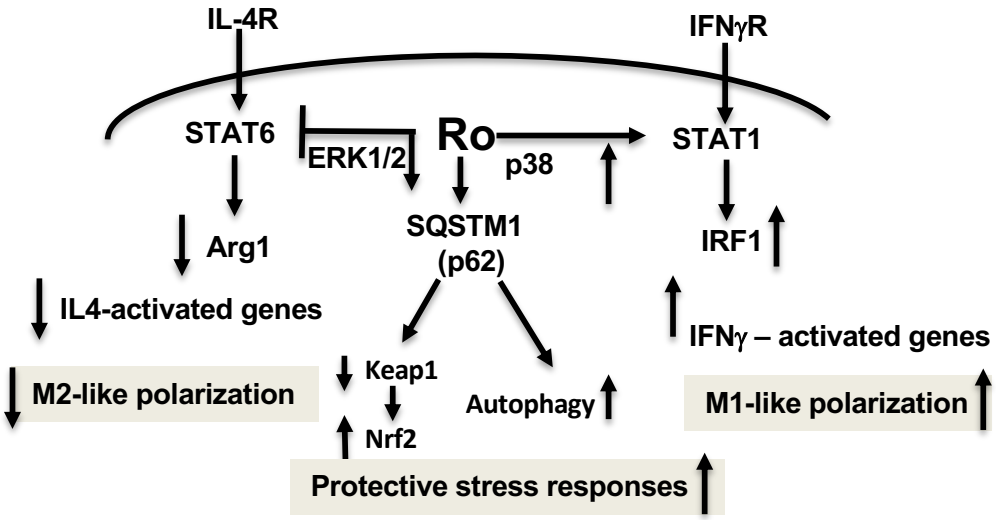
IL-4R
IFNγR
STAT6
ERK1/2
Ro
p38
STAT1
Arg1
SQSTM1
(p62)
IRF1
IL4-activated genes
IFNγ – activated genes
Keap1
M2-like polarization
Autophagy
M1-like polarization
Nrf2
Protective stress responses

Fig.6